# UV spectral filtering by surface structured multilayer mirrors

Qiushi Huang,[1,3,*] Daniel Mathijs Paardekooper,[2] Erwin Zoethout,[1] V. V. Medvedev,[1] Robbert van de Kruijs,[1,3] Jeroen Bosgra,[1] Eric Louis,[1,3] and Fred Bijkerk[1,3]

[1]Dutch Institute for Fundamental Energy Research, P.O. Box 1207, NL-3430BE Nieuwegein, The Netherlands

[2]Sackler Laboratory for Astrophysics, University of Leiden, P.O. Box 9513, NL-2300 RA Leiden, The Netherlands

[3]MESA+ Institute for Nanotechnology, University of Twente, P.O. Box 217, NL-7500AE Enschede, The Netherlands

*Corresponding author: q.huang@utwente.nl

Received November 27, 2013; revised January 17, 2014; accepted January 20, 2014; posted January 22, 2014 (Doc. ID 202112); published February 21, 2014

A surface structured extreme ultraviolet multilayer mirror was developed showing full band suppression of UV ($\lambda = 100$–$400$ nm) and simultaneously a high reflectance of EUV light ($\lambda = 13.5$ nm). The surface structure consists of Si pyramids, which are substantially transparent for EUV but reflective for UV light. The reflected UV is filtered out by blazed diffraction, interference, and absorption. A first demonstration pyramid structure was fabricated on a multilayer by using a straightforward deposition technique. It shows an average suppression of 14 times over the whole UV range and an EUV reflectance of 56.2% at 13.5 nm. This robust scheme can be used as a spectral purity solution for all XUV sources that emit longer wavelength radiation as well. 

*OCIS codes:* (340.7480) X-rays, soft x-rays, extreme ultraviolet (EUV); (310.6188) Spectral properties; (050.1970) Diffractive optics.

http://dx.doi.org/10.1364/OL.39.001185

High reflectivity multilayer mirrors (MLMs) are of particular importance in the EUV and x-ray region (XUV, $\lambda = 40$–$0.1$ nm), since they enable the reflection of this short-wavelength light. They are widely applied in extreme UV photolithography, synchrotron radiation facilities, and high-energy astronomical observations to select the target wavelength with high efficiency. However, many of the XUV sources currently used or investigated in these areas, such as plasma sources [1], solar irradiation [2], and high harmonics generation [3], have a wideband emission spectrum. The spectrum usually contains, apart from the target XUV band, also out-of-band radiation, which can extend to the UV or the visible region. Moreover, these undesired wavelengths can be highly reflected by a single layer, which makes it difficult to be filtered out by a standard MLM. One notable example is EUV lithography ($\lambda_{EUV} = 13.5$ nm) for manufacturing at the sub-22-nm half-pitch node in semiconductor industry [4]. The typical laser produced Sn-plasma EUV source emits a large amount of UV radiation ($\lambda = 100$–$400$ nm) [5], and part of the infrared light from the drive laser is also scattered by the plasma [6]. All this out-of-band radiation will be reflected by the Mo/Si multilayer, causing imaging contrast loss and heat load problems. Therefore, the spectral purity of the source has become one of the challenges for applying EUV lithography in high volume manufacturing [7].

In this Letter, we focus on UV spectral purity problem while the IR filtering can be found in other references [8–11]. Different methods have been developed to suppress the out-of-band UV radiation in the reflected spectrum, including multilayer gratings [12,13], antireflection layers [14,15], and freestanding membranes/filters [16,17]. However, these methods either cannot suppress the whole band of UV light, or a large amount of EUV power is lost due to the added structures. A full-band UV suppression with minimum loss of EUV is required for lithography at high volume production. Here we introduce a new scheme for EUV spectral purity enhancement based on diffracting pyramid structures placed at the multilayer surface.

At near normal incidence, the 13.5 nm EUV light can only be reflected by a periodic multilayer, usually Mo/Si, while UV light is reflected by a single Mo or Si layer of a few nanometer thickness. Si has very low absorption for EUV due to its absorption edge at $\lambda = 12.4$ nm. This opens up the way for a micron-scale tapered surface structure made from pure Si that can scatter or diffract the UV light out of the specular direction while the EUV light is transmitted and reflected by the multilayer underneath. Different tapered structures can be used, including the blazed grating and the pyramid, which can in principle achieve similar suppression effects. Due to the ease of fabrication described below, periodic pyramids with symmetric facets were selected to act as the UV filtering structure, as shown in Fig. 1(a). Two-dimensional pyramids were particularly chosen instead of the 1D ridge-like structures since the former one has less silicon and therefore absorbs less EUV light. The proof of straightforward fabrication and the effective operation is described in the following sections.

To explore this new diffraction structure and obtain the highest UV suppression effect, all structural parameters shown in Fig. 1(b) were explored, including the lateral period of each unit ($p$), the pyramid height ($h$),

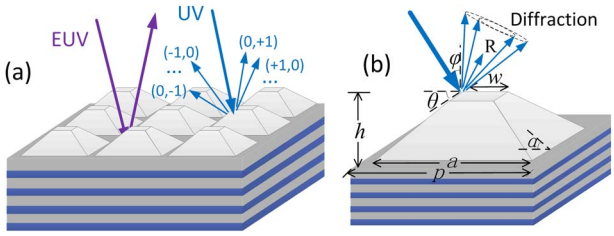


Fig. 1. (a) Schematic of the pyramids-on-ML system. (b) Structural parameters of a single pyramid unit.

 

the width of the top flat area ($w$), and the bottom width of each pyramid ($a$). The tilt angle ($\alpha$) of the facets is defined as $\alpha = \arctan(2h/(a-w))$. The diffraction efficiency of this 3D structure (including the multilayer underneath) is simulated using the DiffractMOD software (Rsoft) based on the rigorous coupled wave analysis [18].

Height is a first critical parameter to impact the suppression effect. Figure 2 shows the simulated UV reflectance of pyramids at normal incidence with $h = 50$, 100, 150, and 220 nm. The period was chosen as $p = 26$ μm (for easy fabrication) with $a = p$, $w = 0$. The total reflectance of each structure (defined as the sum of the efficiency of all diffraction orders including the zeroth-order) and the standard Mo/Si ML reflectance are also shown. These structural parameters represent a shallow pyramid with no top flat area on the ML surface. For this type of pyramid structure, the suppression of UV reflectance comes from two principles: absorption of Si and more dominantly the "blazed" diffraction. The total UV reflectance of the pyramid-ML system is smaller than that of a standard multilayer, and it decreases with increasing height. This is caused by the increased absorption as the light is diffracted forward and back through the thick Si structure (considering the reflection from the ML). Moreover, the zeroth-order reflectance is much smaller than the total $R$, and it drops even faster with larger height. At a height of 220 nm, the UV reflectance is below 3% over the entire wavelength range. This substantial suppression of UV is caused by the blazed diffraction effect of the pyramid, which shifts most of the incident power to higher diffraction orders. The diffraction angles increase with wavelength according to the grating equation, $p(\sin\varphi - \sin\beta) = k\lambda$, $\varphi$ being the incident angle, $\beta$ the diffraction angle, and $k$ the diffraction order. With larger height, the blaze angle ($a$) is increased, which better matches the specular reflection angle (from the facet) with the diffraction angles especially at longer wavelengths. Thus more incident power can be shifted, and lower UV reflectance is achieved over the entire range.

It is worth noting that the reflected power from the facets is distributed into a broader angular region (within several orders) around the specular reflection direction of the facet, compared to a blazed grating. This is due to the 2D symmetric shape of the pyramid structure. In this case, the specular reflection direction from the facets needs to be matched at least to the second diffraction order to reach a decent suppression effect. To limit the absorption of EUV light, the height of the Si pyramid was chosen as $h = 100$ nm.

A top flat area is the second critical parameter found to determine the suppression effect. The UV reflectance of 100 nm height pyramid systems with top-flat width $w = 0$, $0.3p$, and $0.6p$, ($a = p$) were simulated at normal incidence, and the results are shown in Fig. 3. The UV reflectance decreases with larger top flat area especially at the longer wavelength range, but a local maximum in the $R$ curve appears around $\lambda = 160$ nm. The decreased reflectance is caused by two facts. First, the larger top flat area increases the tilt angle of the facets, which helps to shift the incident power to higher orders. Second, light reflected from the top flat area and from the valley part between pyramids interfere with each other, and, given the pyramid height ($h = 100$ nm), there is a destructive interference at the longer wavelength, which helps to further decrease the reflectance. Meanwhile, a constructive interference also occurs at a shorter wavelength, which causes the local maximum in Fig. 3. The wavelength where the local maximum in reflectance appears is smaller than $\lambda = 2h_{\text{pyra}}$. due to the fact that the bottom reflection partly comes from the tapered facets. As $w \geq 0.6p$, the constructive interference becomes so strong that it destroys the suppression effect. The discontinuity of $R$ around $\lambda = 110$ nm can be caused by the abrupt change of Si refractive index. The bottom width of the pyramid (a) determines the cover fraction of the ML surface with the pyramid structure, $(a/p)^2$. It can enhance both interference effects mentioned above by exposing more ML surface, $(a/p)^2 < 1$. The reflectance of pyramids with top-flat width $w = 0.3p$ and $a = 0.9$ p is shown in Fig. 3 (blue curve). Compared to the one with $a = p$ (red curve), the reflectance of longer wavelength is further decreased to below 12% while the local maximum also increases. It is noticed that the local maximum position is now closer to the wavelength of $\lambda = 2h_{\text{pyra.}} =$ 200 nm, as the flat valley area is increased. If the top-flat and valley area are set as $w = a$ and $(w/p)^2 = 0.5$, the pyramid structure is turned into a phase-shift grating [13].

The lateral scale (period) of the pyramid structure is not a sensitive parameter for suppression. Within the range of $p = 1$–50 μm, the lowest UV reflectance achievable is the same for different scales. This is easy to understand, as the period only determines the diffraction angle while the facet angle and top/valley area can be adjusted to shift the UV power to certain orders. A smaller period will make the pyramid work out of the diffraction regime

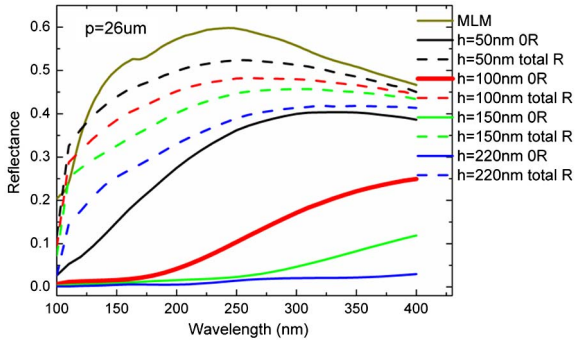


Fig. 2. UV reflectance of pyramid-on-ML system with different height.

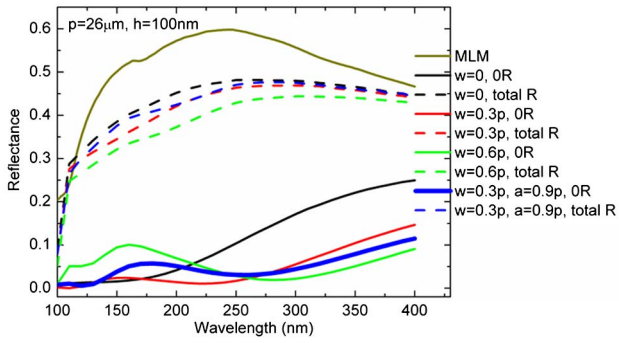


Fig. 3. UV reflectance of pyramids-on-ML system with different top-flat and bottom widths.

of UV light, which is out of the scope of this Letter. For even larger periods, the diffracted UV light is so close to reflection (angular separation between reflection and ±1st order is ~0.1 deg at $\lambda = 100$ nm, $p = 50$ μm), which can make it difficult to separate the bands in practical applications. Due to its 2D symmetric structure, the suppression effect is also not sensitive to the out-of-plane incidence angle ($\theta$) and polarization (around normal incidence). Although the reflectance will increase with larger in-plane incidence angle ($\varphi$), the average reflectance of unpolarized light over the whole UV band can still be below 8% for $\varphi \leq 40$ deg. Based on the simulations, the EUV reflectance of the pyramid-coated ML with $h = 100$ nm, $w = 0.3p$, $a = 0.9p$ is only 11% (relative) less than the standard ML. This is mainly caused by the Si absorption since EUV diffraction from Si pyramids is negligible. Thus this 3D Si pyramid-ML structure shows a very high suppression effect over the whole UV band with only a minor loss of EUV intensity. A proof of principle pyramid structure was designed with parameters listed in Table 1.

To fabricate the Si pyramid structure, a simple deposition method was used, known as the half-shadowing technique. Deposition through a mask (consisting of slits or holes) can produce a gradient of the arriving-particle flux within each half period of the mask structure. It has been used to control the layer thickness profile and make thin film micro-optics [19,20]. In the shadowing deposition, the mean free path of the particles needs to be larger than the target-substrate distance implying a line-of-sight deposition process. Different physical vapor deposition methods, either evaporation or sputtering can be optimized to satisfy this condition. However, sputtering systems usually work at relatively high vacuum pressure [21]. The target-substrate distance has to be limited and the impact from an extended target source is more obvious. Thus an e-beam evaporation system was used in this work. Fifty bilayers Mo/Si with a period of 6.95 nm were deposited on the Si substrate in advance. A commercial 2D fine grid was used as the mask. The open width of each square aperture is $17.2 \pm 0.3$ μm, and the line width is $8.7 \pm 0.3$ μm (period = ~25.9 μm). The grid thickness is only 2–5 μm. It was mounted above the ML substrate at a distance of 200–800 μm to explore the shadowing effect and optimize the shape of the deposited structure. After deposition, the precise shape of the structure was characterized by an atomic force microscope (AFM) as shown in Fig. 4.

The measured structural parameters are listed in Table 1. Based on the AFM results, a pyramid structure with period of 25.9 μm and height of 100 nm was successfully fabricated. It is noted that the AFM image has been rescaled in $x$ and $y$ axis, while the real shape of the pyramid is extremely shallow with a blaze angle of only ~0.8 deg.

**Table 1. Structural Parameters of the Pyramid**

| | Period (μm) | Height (nm) | Top_$w$ (μm) | Bottom_$w$ (μm) |
|---|---|---|---|---|
| Design | 26 | 100 | $0.3p = 7.8$ | $0.9p = 23.4$ |
| Fabrication | 25.9 | 100 | 9.0 | 23.9 |

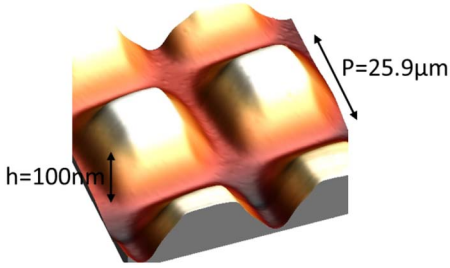


Fig. 4. AFM image of the fabricated pyramids.

The UV and EUV reflectance were measured at the Physikalisch-Technische Bundesanstalt (PTB) in Berlin. During the UV measurement, the incident beam had a divergence of 0.4 deg and a 0.5 mm aperture was used in front of the detector in order to separate the diffraction orders and the reflection from the pyramids. The UV reflectance of the pyramid-ML structure, and a standard ML were both measured at 5° incidence angle, and the results are shown in Fig. 5. Over the whole wavelength range, the reflectance of the pyramids-coated ML was greatly suppressed to 0.1%–10.5% from 100 to 400 nm. Comparing the mean reflectance of a standard ML (52.9%) with the pyramid-ML structure (3.8%) shows that an average suppression factor of 14 was achieved over the entire range. Moreover, a maximum suppression factor of >300 was obtained at $\lambda = 122$ nm, as can be seen from the logarithmic scale plot in the insertion. This sharp minimum is mainly caused by destructive interference effect. The wavelength position of this maximum suppression can be tuned by changing the pyramid height. It can be used to suppress some strong emission line in the spectrum. The simulated reflectance curve using the parameters obtained by AFM fits very well with the measured result indicating a correct theoretical model and accurate structural characterization. Thus a full-band UV suppression device based on diffraction pyramids has been demonstrated.

EUV reflectance was measured at the uncoated and pyramid-coated ML area on the same sample. The incident angle was 1.5 degree off normal, and the results are shown in Fig. 6. The peak reflectance of the uncoated standard ML is 68.3% while the Si pyramids-on-the ML sample shows a reflectance of 56.2%. The EUV "transmittance" at 13.5 nm of this system is defined as $R_{\text{pyra.}}/R_{\text{ML}} = 82.2\%$, significantly higher than the free-

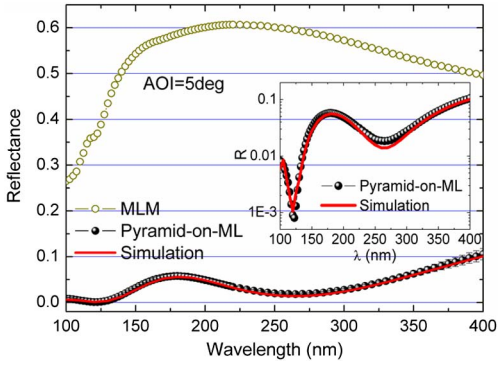


Fig. 5. Measured UV reflectance of the pyramid-on-ML system and the MLM. The reflectance curve in log scale is shown in the insertion.

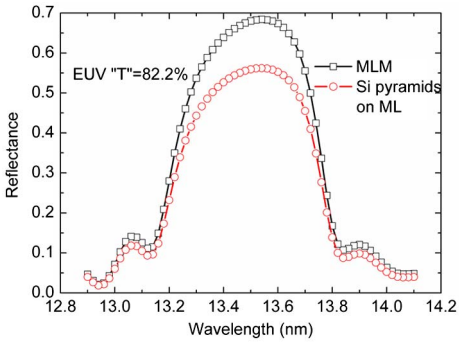


Fig. 6. Measured EUV reflectance of the pyramid-on-ML system and the MLM.

standing membranes [16]. As the pyramids are made of Si, which is almost nonreflective for EUV radiation, the diffraction and scattering of EUV light can be neglected. By using a slit, e.g., at the image plane of the mirror, the UV diffraction can be blocked, resulting in transmission of the EUV part of the spectrum only. The larger drop of EUV reflectance compared to theory (theoretical "transmittance" $R_{\text{pyra.}}/R_{\text{ML}} = 89\%$) is caused by absorption for several reasons: the fabricated top-flat and bottom width are larger than designed, and the amount of Si deposited is slightly larger than the volume of the 100 nm pyramid (~5 nm thickness excess layer at the bottom of pyramids) due to imperfections of the shadow deposition process. Furthermore, the surface Si oxidized into $SiO_2$ of typically ~2 nm thickness [22] and covered the whole surface area of the pyramids.

To further improve the EUV reflectance, the source emission spectrum can be taken into account during the pyramid design. The Si pyramids fabricated here exhibit a high suppression effect over the whole band. However, the maximum integral suppression needed depends on the amount of UV power generated in the plasma source and its spectral distribution [23]. Relatively higher UV reflectance at certain wavelengths may be acceptable, i.e., less height or top-flat width of pyramid is required and thus more EUV power can be gained back.

In summary, a novel micron-scale diffraction pyramid structure integrated with short-wavelength reflecting MLMs was designed and demonstrated using a straightforward fabrication process. Based on the combined effects of blazed diffraction, interference, and absorption, the first Si pyramid-ML system shows an average UV suppression of 14 times in the band from $\lambda = 100$ to 400 nm and a maximum suppression factor of >300 at a specific wavelength. The EUV reflectance of this prototype is 56.2% at 13.5 nm. To the best knowledge of the authors, this is the first time that a multilayer-based structure can achieve such a full band suppression through the entire UV range and maintain high EUV reflectance. The structure of the pyramids can be optimized to further reduce the EUV loss. Due to the simple blazed diffraction and interference effects, the pyramid scheme can be easily applied to other wavelength range and applications such as high harmonics generation source or astronomical observation to suppress the long-wavelength background.

The authors are grateful to Dr. Alexander Gottwald and Dr. Christian Laubis at the Physikalisch Technische Bundesanstalt (PTB) in Berlin for the UV and EUV measurements. This work is part of the research program "Controlling photon and plasma induced processes at EUV optical surfaces (CP3E)" of the Stichting voor Fundamenteel Onderzoek der Materie. The CP3E program is co-financed by Carl Zeiss SMT GmbH (Oberkochen), ASML (Veldhoven), and the AgentschapNL through the Catrene EXEPT program.

## References

1. V. Y. Banine, K. N. Koshelev, and G. H. P. M. Swinkels, J. Phys. D **44**, 253001 (2011).
2. J. Lilensten, T. Dudok de Wit, M. Kretzschmar, P.-O. Amblard, S. Moussaoui, J. Aboudarham, and F. Auchère, Ann. Geophys. **26**, 269 (2008).
3. J. Seres, E. Seres, A. J. Verhoef, G. Tempea, C. Streli, P. Wobrauschek, V. Yakovlev, A. Scrinzi, C. Spielmann, and F. Krausz, Nature, **433**, 596 (2005).
4. C. Wagner and N. Harned, Nat. Photonics, **4**, 24 (2010).
5. I. V. Fomenkov, D. C. Brandt, A. N. Bykanov, A. I. Ershov, W. N. Partlo, D. W. Myers, N. R. Böwering, G. O. Vaschenko, O. V. Khodykin, J. R. Hoffman, E. Vargas, R. D. Simmons, J. A. Chavez, and C. P. Chrobak, Proc. SPIE **6517**, 65173J (2007).
6. J. Fujimoto, T. Hori, T. Yanagida, T. Ohta, Y. Kawasuji, Y. Shiraishi, T. Abe, T. Kodama, H. Nakarai, T. Yamazaki, and H. Mizoguchi, Proc. SPIE **8332**, 83220F (2012).
7. R. Moors, V. Banine, G. Swinkels, and F. Wortel, J. Micro/Nanolithogr. MEMS MOEMS **11**, 021102 (2012).
8. V. V. Medvedev, A. J. R. van den Boogaard, R. van der Meer, A. E. Yakshin, E. Louis, V. M. Krivtsun, and F. Bijkerk, Opt. Express, **21**, 16964 (2013).
9. V. V. Medvedev, A. E. Yakshin, R. W. E. van de Kruijs, V. M. Krivtsun, A. M. Yakunin, K. N. Koshelev, and F. Bijkerk, Opt. Lett. **37**, 1169 (2012).
10. M. Trost, S. Schröder, A. Duparré, S. Risse, T. Feigl, U. D. Zeitner, and A. Tünnermann, Opt. Express, **21**, 27852 (2013).
11. W. A. Soer, P. Gawlitza, M. M. J. W. van Herpen, M. J. J. Jak, S. Braun, P. Muys, and V. Y. Banine, Opt. Lett. **34**, 3680 (2009).
12. J. Alexander Liddle, F. Salmassi, P. P. Naulleau, and E. M. Gullikson, J. Vac. Sci. Technol. B **21**, 2980 (2003).
13. A. J. R. van den Boogaard, F. A. van Goor, E. Louis, and F. Bijkerk, Opt. Lett., **37**, 160 (2012).
14. M. M. J. W. van Herpen, R. W. E. van de Kruijs, D. J. W. Klunder, E. Louis, A. E. Yakshin, S. Alonso van der Westen, F. Bijkerk, and V. Banine, Opt. Lett. **33**, 560 (2008).
15. S. P. Huber, R. W. E. van de Kruijs, A. E. Yakshin, E. Zoethout, and F. Bijkerk, Proc. SPIE **8848**, 884814 (2013).
16. N. I. Chkhalo, M. N. Drozdov, E. B. Kluenkov, A. Y. Lopatin, V. I. Luchin, N. N. Salashchenko, N. N. Tsybin, L. A. Sjmaenok, V. E. Banine, and A. M. Yakunin, J. Micro/Nanolithogr. MEMS MOEMS **11**, 021115 (2012).
17. I. A. Artyukov, A. I. Fedorenko, V. V. Kondratenko, S. A. Yulin, and A. V. Vinogradov, Opt. Commun. **102**, 401 (1993).
18. M. G. Moharam and T. K. Gaylord, J. Opt. Soc. Am. **73**, 451 (1983).
19. S. K. Yao, J. Appl. Phys. **50**, 3390 (1979).
20. R. Grunwald, U. Neumann, U. Griebner, G. Stibenz, S. Langer, G. Steinmeyer, V. Kebbel, and M. Piché, Proc. SPIE **5827**, 187 (2005).
21. D. M. Mattox, *Handbook of Physical Vapor Deposition (PVD) Processing: Film Formation, Adhesion, Surface Preparation and Contamination Control* (Noyes, 1998).
22. W. M. Clift, L. E. Klebanoff, C. Tarrio, S. Grantham, O. R. Wood II, S. Wurm, and N. V. Edwards, Proc. SPIE **5374**, 666 (2004).
23. I. V. Fomenkov, D. C. Brandt, N. R. Farrar, B. La Fontaine, N. R. Böwering, D. J. Brown, A. I. Ershov, and D. W. Myers, Proc. SPIE **8679**, 86792I (2013).